9. Stress evaluation in combined immersed boundary lattice Boltzmann simulations

The recovery of the stress tensor in computer simulations is not as straight-forward as it may appear at first view. The reason is that usually not the stress tensor $\boldsymbol{\sigma}$ itself enters the macroscopic equations. Rather, its divergence, $\nabla \cdot \boldsymbol{\sigma}$ appears. Even if this divergence is known, it is generally not possible to uniquely reconstruct the stress tensor from it since the equation system is underdetermined[1]. It has already been mentioned in section 5.2 that the full fluid stress tensor is known at each point within the lattice Boltzmann method (LBM). The situation is different for the particle stress. If, however, averages of some kind are sufficient (e.g., over time, volume, or a coordinate plane), different approaches are available to recover the particle stress tensor or some of its components.

In this chapter, it is argued how suspension stresses can be evaluated within the model presented in the previous chapters. The discussion is limited to viscous flows where inertia effects are negligible. The fluid stress considerations are briefly summarized in section 9.1, followed by the wall stress in section 9.2. The direct recovery of particle stresses is more demanding as discussed in sections 9.3 and 9.4. Verification simulations are presented in section 9.5, linking the above approaches.

9.1. Fluid stress evaluation in the lattice Boltzmann method

Simple fluids cannot support elastic stresses, and the fluid stress equals the viscous stress [2],

$$\boldsymbol{\sigma}^{\mathrm{f}} = 2\eta_0 \boldsymbol{S}, \tag{9.1}$$

where $S_{\alpha\beta} = \frac{1}{2}(\partial_\alpha u_\beta + \partial_\beta u_\alpha)$, cf. eq. (2.5), are the components of the symmetric fluid shear rate tensor and η_0 is the dynamic shear viscosity. Bulk stresses due to compressibility effects are neglected here and in the following.

For a Newtonian fluid, the dynamic shear viscosity does not depend on the shear rate, and the stress is proportional to the shear rate. Water and blood plasma are examples of Newtonian fluids over a wide range of shear rates, including physiological shear rates up to about $10^4\,\mathrm{s}^{-1}$. The fluid described in the standard LBM is Newtonian as long as the relaxation parameter τ is a constant. Although LBM extensions for non-Newtonian fluids exist (e.g., [229, 230, 231]), the suspending fluid is always Newtonian in the present work. Non-Newtonian suspension rheology emerges from the presence of particles immersed in the fluid.

For conventional Navier-Stokes solvers where the Navier-Stokes equations (NSE) are directly discretized, the fluid stress is usually computed from the velocity field via differentiation. In lattice Boltzmann simulations, however, the full fluid stress tensor is accessible at each point and without evaluating velocity gradients, cf. eq. (5.17). This makes the LBM an attractive Navier-Stokes solver when the rheology of fluids is to be investigated.

[1] The divergence $\nabla \cdot \boldsymbol{\sigma}$ yields three equations, but six independent components of the symmetric stress tensor $\boldsymbol{\sigma}$ are required.

T. Krüger, *Computer Simulation Study of Collective Phenomena in Dense Suspensions of Red Blood Cells under Shear,* DOI 10.1007/978-3-8348-2376-2_9,

9.2. Wall stress evaluation in the lattice Boltzmann method

The wall stress tensor $\boldsymbol{\sigma}^{\mathrm{w}}$ is related to the total force $\Delta \boldsymbol{p}/\Delta t$ acting on a small patch of the oriented wall surface $\Delta \boldsymbol{A}$ in a given time Δt as defined in eq. (5.28),

$$\frac{\Delta \boldsymbol{p}}{\Delta t} = \boldsymbol{\sigma}^{\mathrm{w}} \cdot \Delta \boldsymbol{A}, \tag{9.2}$$

where $\Delta \boldsymbol{p}$ is the corresponding momentum exchange in time Δt. In the present work, only the shear components are considered. They are caused by the force components parallel to the wall, $\Delta \boldsymbol{p}_{\parallel} \cdot \Delta \boldsymbol{A} = 0$.

For a suspension, the wall stress is the sum of the fluid stress and the particle stress at the wall. Due to lubrication effects and hydrodynamic lift forces, particles are usually in no direct contact with a wall [227], and $\Delta \boldsymbol{p}/\Delta t$ is the force due to the momentum exchange of the fluid caused by the no-slip boundary condition. Within the LBM, the wall stress can be evaluated at each surface patch $\Delta \boldsymbol{A}$ from eq. (5.27).

If the walls are made rough as discussed in section 8.8, the stick forces have to be considered in the computation of the wall stress, and the total force acting on the entire wall is the sum of the fluid forces and the negative of the stick forces ('actio = reactio') as defined in eq. (8.17).

For steady and simple shear flow, the condition of mechanical stability demands that the wall shear stresses at the bottom and top walls are identical and equal to the shear stress everywhere else in the system. For this reason, an evaluation of the wall stress is in principle sufficient if the total suspension stress and the average viscosity are to be computed. This is the approach commonly followed in rheology experiments. However, it does not allow the local separation of fluid and particle stresses, and, therefore, the local viscosity between the walls cannot be accessed. In some cases, the local stresses are of high relevance, especially if wall effects are important and the system is not homogeneous [5]. It is desirable to measure the contributions of the fluid and the particles to the total stress locally and *independently*. In experiments, a local stress measurement is extremely difficult if not impossible. Even in simulations, it is not a priori clear how to evaluate local particle stresses. Two possible approaches are presented in the following sections.

9.3. Evaluating particle stresses with Batchelor's approach

In a simple fluid, the stress $\boldsymbol{\sigma}$ is of viscous nature only, and one can write $\boldsymbol{\sigma} = 2\eta_0 \boldsymbol{S}$ at each point in the fluid. If particles—deformable or not—are suspended in this fluid, there are additional stress contributions caused by the distorted velocity field due to the presence of the particles. In the following, only the shear component (xz-component) of the stress in simple shear flows (velocity along x-axis, velocity gradient along z-axis) is considered. All other stress components are either not relevant for the present discussion, or they vanish on average. The apparent viscosity is defined via the volume average

$$\langle \sigma_{xz} \rangle_V = 2\eta_{\mathrm{app}} \langle S_{xz} \rangle_V. \tag{9.3}$$

Suspension stress

It is possible to compute the apparent viscosity for a dilute suspension of rigid, spherical particles in simple shear flow [2, 14]. The Einstein relation states that, for a volume fraction ϕ not larger than a few percent, the apparent viscosity is $\eta_{\mathrm{app}} = \eta_0 \left(1 + \frac{5}{2}\phi\right)$, cf. section 2.3. For arbitrary volume fractions and general particle shapes and deformabilities, it is either extremely difficult

or even impossible to find the apparent viscosity analytically. Instead, numerical approaches may be required.

In his seminal work, Batchelor [10] derived a general, formal expression for the stress in suspensions subject to shear flow. Starting from the NSE, Batchelor first introduced the *bulk stress* including pressure,

$$\boldsymbol{\Sigma} := \langle -p\boldsymbol{I} + \boldsymbol{\sigma} \rangle_V = \frac{1}{V} \int \mathrm{d}V \, (-p\boldsymbol{I} + \boldsymbol{\sigma}), \tag{9.4}$$

as the volume average of the local stress. At this point, locality is already lost. It has been further shown that the bulk stress can be written in the form

$$\boldsymbol{\Sigma} = -\frac{1}{V} \int_{\text{fluid}} \mathrm{d}V \, p\boldsymbol{I} + 2\eta_0 \langle \boldsymbol{S} \rangle_V + \langle \boldsymbol{\sigma}^{\text{p}} \rangle_V \tag{9.5}$$

where the pressure is only integrated over the fluid volume (volume not occupied by particles). This isotropic pressure contribution is not of interest here, and it is neglected in the following. As can be inferred from eq. (9.5), the total stress can be written as the sum of the *known* fluid stress $2\eta_0 \langle \boldsymbol{S} \rangle_V$ as it would be in the absence of the particles and the particle stress $\langle \boldsymbol{\sigma}^{\text{p}} \rangle_V$. Exploiting Gauss' theorem, the particle stress can be shown to have the components

$$\langle \sigma^{\text{p}}_{\alpha\beta} \rangle_V = \frac{1}{V} \sum_k \oint_{A_k} \mathrm{d}A \, \left(S_{\alpha\gamma} x_\beta n_\gamma - \eta_0 (u_\alpha n_\beta + u_\beta n_\alpha) \right). \tag{9.6}$$

The sum runs over all suspended particles, and the integration is taken over particle surfaces with the unit normal vector $\boldsymbol{n}$ pointing into the fluid[2]. $\boldsymbol{x}$ is the position vector with an arbitrary origin. Eq. (9.5) and eq. (9.6) are generally valid for negligible inertia effects and for a Newtonian suspending fluid at any instance of time. The particle shape and the volume fraction ϕ are not restricted in any form.

Application to immersed elastic membranes

In the following, the above formalism will be applied to thin membranes immersed in a fluid. These membranes are filled with another Newtonian fluid of viscosity $\lambda\eta_0$ where λ is the viscosity ratio. In this case, both the exterior and the interior surfaces have to be considered, and one can write

$$\begin{aligned} \langle \sigma^{\text{p}}_{\alpha\beta} \rangle_V = &\frac{1}{V} \sum_k \oint_{A_k^+} \mathrm{d}A \, \left(S_{\alpha\gamma} x_\beta n^+_\gamma - \eta_0 (u_\alpha n^+_\beta + u_\beta n^+_\alpha) \right) \\ &+ \frac{1}{V} \sum_k \oint_{A_k^-} \mathrm{d}A \, \left(S_{\alpha\gamma} x_\beta n^-_\gamma - \lambda\eta_0 (u_\alpha n^-_\beta + u_\beta n^-_\alpha) \right). \end{aligned} \tag{9.7}$$

Each membrane has an exterior and an interior surface which are denoted by $+$ and $-$, respectively. Thus, A^+ lies in the exterior fluid with viscosity η_0 and A^- in the interior fluid with viscosity $\lambda\eta_0$. Due to the small thickness of the membrane, both surfaces have an infinitesimal distance ϵ from each other, and the normal vectors $\boldsymbol{n}^+$ and $\boldsymbol{n}^-$ pointing into the exterior and the interior fluid obey $\boldsymbol{n}^+ = -\boldsymbol{n}^-$. Since the velocity $\boldsymbol{u}$ is smooth at the membrane surface (no-slip condition), the particle stress can be written in the form

$$\langle \sigma^{\text{p}}_{\alpha\beta} \rangle_V = \frac{1}{V} \sum_k \left(\oint_{A_k^+} - \oint_{A_k^-} \right) \mathrm{d}A \, S_{\alpha\gamma} x_\beta n_\gamma + \frac{1}{V} \sum_k \oint_{A_k} \mathrm{d}A \, (\lambda - 1) \eta_0 (u_\alpha n_\beta + u_\beta n_\alpha) \tag{9.8}$$

[2] The integration is performed in the exterior fluid, directly outside of the suspended particles where fluid velocity and shear rate are defined.

where $\boldsymbol{n} = \boldsymbol{n}_+ = -\boldsymbol{n}_-$ has been substituted. Tensions in the membrane are balanced by a jump of the fluid stress across the interface [129], and

$$\tilde{\boldsymbol{f}} = (\boldsymbol{S}^- - \boldsymbol{S}^+) \cdot \boldsymbol{n} \tag{9.9}$$

holds where $\boldsymbol{S}^+$ and $\boldsymbol{S}^-$ are the values of the fluid stress tensor directly outside and inside of the membrane, respectively. The force density $\tilde{\boldsymbol{f}}$ (force per area) is exerted *on the fluid* by the membrane[3], and for a given membrane deformation it is known from the constitutive model, cf. chap. 7. Consequently, the particle stress is [25]

$$\langle \sigma^{\mathrm{p}}_{\alpha\beta} \rangle_V = \frac{1}{V} \sum_k \oint_{A_k} \mathrm{d}A \left(-\tilde{f}_\alpha x_\beta + (\lambda - 1)\eta_0 (u_\alpha n_\beta + u_\beta n_\alpha) \right). \tag{9.10}$$

In the present work, the interior fluid has the same viscosity as the exterior fluid, $\lambda = 1$, and the bulk particle stress reduces to the compact form

$$\langle \sigma^{\mathrm{p}}_{\alpha\beta} \rangle_V = -\frac{1}{V} \sum_k \oint_{A_k} \mathrm{d}A \, \tilde{f}_\alpha x_\beta. \tag{9.11}$$

Remarks

It is straightforward to evaluate eq. (9.11) within the present model. The discretization of eq. (9.11) reads

$$\langle \sigma^{\mathrm{p}}_{\alpha\beta} \rangle_V = -\frac{1}{V} \sum_i F_{i\alpha} x_{i\beta} \tag{9.12}$$

where the sum runs over all Lagrangian membrane nodes i (force $\boldsymbol{F}_i$, position $\boldsymbol{x}_i$) in the entire simulation box. The origin of the coordinate system is arbitrary if the sum of all forces in the system is exactly zero, $\sum_i \boldsymbol{F}_i = 0$. Indeed, the definition of the particle stress in eq. (9.11) is only useful if there is no net force on the particles. Else, the particle stress could take any value by choosing a convenient coordinate origin.

The particle stress as given in eq. (9.11) is the *average* particle stress in the entire system. There is a priori no access to a local particle stress within Batchelor's approach. However, it is possible to compute the contributions of individual particles k,

$$\langle \sigma^{\mathrm{p}}_{k\alpha\beta} \rangle_V := -\frac{1}{V} \oint_{A_k} \mathrm{d}A \, \tilde{f}_\alpha x_\beta. \tag{9.13}$$

This stress may then be considered as being located at the centroid of the particle. It will be shown in section 9.5 that this approach does not give satisfactory results. Moreover, interacting particles lead to problems since for such a system, the net force on an individual particle is not zero in general. Interaction forces should be excluded from eq. (9.13).

9.4. Evaluating local particle stresses with the method of planes

The approach presented in section 9.3 allows to obtain the volume average of the particle stress, $\langle \sigma^{\mathrm{p}}_{\alpha\beta} \rangle_V$. While the fluid stress $\boldsymbol{\sigma}^{\mathrm{f}}$ can be obtained locally (section 9.1), this is not possible for the particle stress up to this point. In principle, the particle stress may be obtained indirectly. For example, it is known that, for a simple shear flow, the shear stress averaged over time

[3] An opposite force is exerted on the membrane by the fluid, which is the reason for contradicting sign conventions often found in the literature.

and the xy-plane is constant throughout the system, $\langle\sigma_{xz}\rangle_{x,y,t} \neq \langle\sigma_{xz}\rangle_{x,y,t}(z)$. The fluid stress $\langle\sigma^{\mathrm{f}}_{xz}\rangle_{x,y,t}(z)$ is known, so the particle stress is

$$\langle\sigma^{\mathrm{p}}_{xz}\rangle_{x,y,t}(z) = \langle\sigma_{xz}\rangle_{x,y,t} - \langle\sigma^{\mathrm{f}}_{xz}\rangle_{x,y,t}(z). \tag{9.14}$$

For a rheological study, this relation may in principle be sufficient. Still, within this approach, there is no access to spatio-temporal fluctuations of the particle stress. These fluctuations carry important additional information about the system, e.g., an independent measure of shear viscosity in the small shear rate regime [232],

$$\eta \propto \int_0^\infty \mathrm{d}t' \, \langle\sigma_{xz}(0)\sigma_{xz}(t')\rangle_V. \tag{9.15}$$

In this section, another approach for the particle stress evaluation is presented (Krüger et al. [233]). It offers the possibility to find the *instantaneous and local* particle stress on a plane parallel to the confining walls. For a special case, this technique is shown to be identical to the 'method of planes' (MOP) which has been introduced by Todd et al. [4] for the case of a simple liquid and further examined by Varnik et al. [5] in the case of a polymer melt.

Without external forces, the NSE can be written as

$$\boldsymbol{g}(\boldsymbol{r},t) = \nabla\cdot\boldsymbol{\sigma}(\boldsymbol{r},t) \tag{9.16}$$

where $\boldsymbol{g}$ contains the convective derivative of the velocity and the pressure gradient. In the present model, however, the lattice Boltzmann stress tensor only captures the fluid component, whereas the particle contribution is contained in the force density $\boldsymbol{f}$,

$$\boldsymbol{g}(\boldsymbol{r},t) = \nabla\cdot\boldsymbol{\sigma}^{\mathrm{f}}(\boldsymbol{r},t) + \boldsymbol{f}(\boldsymbol{r},t). \tag{9.17}$$

Therefore, the first step is to assume that the particle stress and the membrane force density are connected via

$$\boldsymbol{f}(\boldsymbol{r},t) = \nabla\cdot\boldsymbol{\sigma}^{\mathrm{p}}(\boldsymbol{r},t). \tag{9.18}$$

This fundamental relation is local both in space and time and known to be valid for elastic systems in equilibrium, i.e., in the absence of accelerations [189]. Eq. (9.18) states that the effect of interactions on flow behavior can be incorporated in the NSE either by (i) direct implementation of particle forces as a (spatially and temporally varying) external force field or (ii) by introducing the particle stress tensor. For any differentiable stress field $\boldsymbol{\sigma}^{\mathrm{p}}(\boldsymbol{r},t)$, a corresponding force density $\boldsymbol{f}(\boldsymbol{r},t)$ can be obtained.

Stress evaluation

The α-component of eq. (9.18) can be written as

$$f_\alpha(\boldsymbol{r},t) = \partial_x\sigma^{\mathrm{p}}_{\alpha x}(\boldsymbol{r},t) + \partial_y\sigma^{\mathrm{p}}_{\alpha y}(\boldsymbol{r},t) + \partial_z\sigma^{\mathrm{p}}_{\alpha z}(\boldsymbol{r},t). \tag{9.19}$$

For periodic boundary conditions along the x- and y-axes, as in the present work, and averaging over the xy-plane, this equation simplifies to

$$\langle f_\alpha\rangle_{x,y}(z,t) = \partial_z\langle\sigma^{\mathrm{p}}_{\alpha z}\rangle_{x,y}(z,t). \tag{9.20}$$

Integration yields

$$\langle\sigma^{\mathrm{p}}_{\alpha z}\rangle_{x,y}(z,t) = \langle\sigma^{\mathrm{p}}_{\alpha z}\rangle_{x,y}(z_0,t) + \int_{z_0}^{z} \mathrm{d}z' \, \langle f_\alpha\rangle_{x,y}(z',t) \tag{9.21}$$

which is a very important intermediate result. It states that, if the force density $\boldsymbol{f}(\boldsymbol{r},t)$ and the xy-average of the particle stress at position z_0 are known, then the xy-average of the particle stress at each z-position is known.

In its discretized form, the force density in the Lagrangian system can be written as

$$\boldsymbol{f}(\boldsymbol{r},t) = \sum_i \boldsymbol{F}_i(t)\delta(\boldsymbol{r} - \boldsymbol{x}_i(t)) \tag{9.22}$$

where $\boldsymbol{F}_i$ is the force acting on Lagrangian node i which is located at point $\boldsymbol{x}_i(t)$ at time t. Interestingly, the particle membership of node i and the physical origin of $\boldsymbol{F}_i$ do not play a role. In particular, it is not necessary to claim that $\boldsymbol{F}_i$ is a two-body force. This is important for multi-body forces which enter $\boldsymbol{F}_i$, e.g., through bending or volume contributions. The discretized form of the particle stress reads

$$\langle\sigma^{\mathrm{p}}_{\alpha z}\rangle_{x,y}(z,t) = \langle\sigma^{\mathrm{p}}_{\alpha z}\rangle_{x,y}(z_0,t) + \frac{1}{A}\sum_i F_{i\alpha}(t)\theta(z_i(t) - z_0)\theta(z - z_i(t)) \tag{9.23}$$

where $A = L_x L_y$ (L_x and L_y being the system extensions along the x- and y-directions) and $\theta(z)$ is the Heaviside step function, i.e., all Lagrangian nodes between z_0 and z contribute.

Method of planes

It will be shown in the following that eq. (9.23) reduces to the equation proposed by Todd et al. [4],

$$\langle\sigma^{\mathrm{p}}_{\alpha z}\rangle_{x,y}(z,t) = -\frac{1}{2A}\sum_i F_{i\alpha}(t)\mathrm{sgn}(z_i(t) - z), \tag{9.24}$$

for some additional assumptions. Here, $\mathrm{sgn}(z)$ is the sign function. The first assumption is that the particle stress vanishes at z_0, $\langle\sigma^{\mathrm{p}}_{\alpha z}\rangle_{x,y}(z_0,t) = 0$, and that no nodes exist with $z_i(t) < z_0$. Thus, z_0 may be taken as the position of the impenetrable bottom wall. The second claim is that the total force vanishes, $\sum_i F_{i\alpha}(t) = 0$, i.e., the total momentum is conserved. This translates to $\sum_i F_{i\alpha}(t)\theta(z - z_i(t)) = -\sum_i F_{i\alpha}(t)\theta(z_i(t) - z)$ and

$$\begin{aligned}\sum_i F_{i\alpha}(t)\theta(z - z_i(t)) &= \frac{1}{2}\left(\sum_i F_{i\alpha}(t)\theta(z - z_i(t)) - \sum_i F_{i\alpha}(t)\theta(z_i(t) - z)\right)\\ &= \frac{1}{2}\sum_i F_{i\alpha}(t)\mathrm{sgn}(z - z_i(t)).\end{aligned} \tag{9.25}$$

Hence, the formal connection between eq. (9.23) and eq. (9.24) has been shown.

Remarks

The MOP [4] has originally been introduced to find the local stress in an atomistic non-equilibrium fluid in planar geometries. Interestingly, it can be applied directly to the present problem by assuming that the deformable membranes consist of interacting point particles. Formally, this is actually the case because the forces acting on the membranes are considered as being concentrated at the Lagrangian nodes. The physical origin of these forces do not play a role at all.

It must be emphasized again that stresses due to inertia effects are not considered here. On the one hand, the fluid inertia is neglected in the NSE in the first place. On the other hand, the equilibrium condition, eq. (9.18), in the absence of accelerations is considered. As will be shown in section 9.5, the MOP produces excellent results for the local particle stress.

The MOP as presented in eq. (9.23) bases on the forces defined in the Lagrangian system. It is also possible to compute the particle stresses in the Eulerian frame by using the lattice force density as obtained from the immersed boundary spreading via eq. (6.5), i.e., the delta function in eq. (9.22) is replaced by the smooth interpolation stencil, e.g., eq. (6.11). For the present model, this second approach will be employed if not otherwise stated. The reason is that the fluid is driven by the forces in the Eulerian system. It is not aware of the presence of the membranes otherwise. This way, both the fluid and the particle stresses are computed in the Eulerian system. Eq. (9.23) then becomes

$$\langle \sigma^{\mathrm{p}}_{\alpha z} \rangle_{x,y}(z,t) = \langle \sigma^{\mathrm{p}}_{\alpha z} \rangle_{x,y}(z_0,t) + \frac{1}{A} \sum_{\boldsymbol{X}'} f_\alpha(\boldsymbol{X}',t) \Delta x^3 \theta(z'-z_0)\theta(z-z') \tag{9.26}$$

where the sum runs over all lattice nodes at position $\boldsymbol{X}' = (x',y',z')$ with force density $\boldsymbol{f}(\boldsymbol{X}',t)$, i.e., the force acting on one lattice unit volume Δx^3 is $\boldsymbol{f}(\boldsymbol{X}',t)\Delta x^3$ (Krüger et al. [233]).

9.5. Benchmark test: verification of the stress evaluation methods

Two classes of benchmark tests have been performed to show (i) the reliability and capability of the stress evaluation methods described in this chapter, (ii) the wall roughening procedure (section 8.8), and (iii) the shear stress boundary condition (section 5.4.2). A single spherical capsule in simple shear flow is considered in section 9.5.1, whereas a dense suspension of spherical capsules (50% volume fraction) is simulated in section 9.5.2. All quantities are given in lattice units.

9.5.1. Single capsule in shear flow

A single spherical capsule ($r = 8$, $N_f = 2000$, $\kappa_{\mathrm{S}} = 0.1$, $\kappa_\alpha = 1$, $\kappa_{\mathrm{B}} = 0.01$, $\kappa_{\mathrm{A}} = 1$, $\kappa_{\mathrm{V}} = 1$) is placed in the middle of an initially quiescent fluid (volume $30 \times 30 \times 30$) bounded by two rigid walls at $z = 0$ and $z = 30$. The LBM relaxation parameter is $\tau = 1$, and the average fluid density is unity. Two simulations for a single particle in shear flow have been performed, one with velocity boundary conditions (VBC), the other with shear stress boundary conditions (SBC).

In the first simulation, both walls are moved along the x-axis in opposite directions with a constant velocity of ± 0.02, resulting in an average fluid shear rate $\langle \dot{\gamma} \rangle_V = 1.33 \times 10^{-3}$. The average fluid stress, therefore, is $\langle \sigma^{\mathrm{f}}_{xz} \rangle_V = 2.22 \times 10^{-4}$, independent of the velocity profile between the walls. The results for the particle stress obtained from the wall stress and Batchelor's approach are shown as function of time in fig. 9.1(a). After an initial transient in which the system is not in steady state, both stresses become equal. The time-averaged particle stress between $t = 4000$ and $t = 10000$ is $\langle \sigma^{\mathrm{p}}_{xz} \rangle_{V,t} = 5.67 \times 10^{-5}$ in both cases. For the average stresses obtained from the MOP, there are slightly different results depending on whether the stress is evaluated in the Eulerian or the Lagrangian frame. In the former, it equals the value obtained before, $\langle \sigma^{\mathrm{p}}_{xz} \rangle_{V,t} = 5.67 \times 10^{-5}$. In the latter, it is slightly larger, $\langle \sigma^{\mathrm{p}}_{xz} \rangle_{V,t} = 5.73 \times 10^{-5}$. The reason for this deviation is caused by the immersed boundary force spreading from the Lagrangian to the Eulerian system. Still, the deviation is only 1%. The curve of the time evolution of the volume-averaged particle stress obtained by the MOP in the Eulerian frame collapses with the curve for Batchelor's stress. For this reason, the MOP stress is not shown separately. This observation is a strong indication for the reliability and consistency of the stress evaluation approaches. The fluid stress, evaluated independently and averaged over time (between $t = 4000$ and 10000) and the total volume, is $\langle \sigma^{\mathrm{f}}_{xz} \rangle_{V,t} = 2.22 \times 10^{-4}$ as expected.

For the second simulation, the walls are subject to the SBC. The prescribed shear stress is 2.79×10^{-4} which is the sum of the fluid and particle stresses obtained from the previous

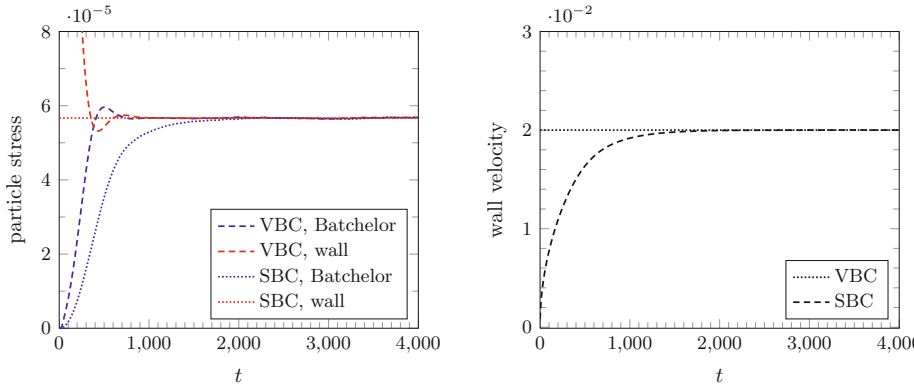

(a) particle stress (b) wall velocity

Fig. 9.1.: Time evolution of particle stress and wall velocity for a single capsule. The results for the velocity boundary condition (VBC) and the shear stress boundary condition (SBC) are compared. The average particle stress $\langle \sigma^{\mathrm{p}}_{xz} \rangle_V$ has been evaluated using (i) Batchelor's approach and (ii) the wall stress (minus the average fluid stress). In steady state, all results are identical. For the VBC, the wall is impulsively accelerated from zero velocity to 0.02, and the resulting wall stress is initially large. For the SBC, the wall is continuously accelerated, and the transient is longer. The slight fluctuations in steady state are caused by the discrete particle mesh.

simulation run in steady state. All other simulation parameters are then same. The most important observation is that, after a transient, both wall velocities become constant with $u^{\mathrm{w}} = 0.02$ as in the first simulation, cf. fig. 9.1(b). All other steady-state stresses are found to be equal, cf. fig. 9.1(a) and fig. 9.2(a). Again, the time evolutions of Batchelor's stress and the volume-averaged MOP stress are identical (MOP stress not shown separately).

Conclusions and remarks

The above discussion clearly shows the consistency of the SBC for a single particle in simple shear flow. After the initial transients, both simulations are equivalent (fig. 9.1 and fig. 9.2). There are some minor fluctuating deviations between the VBC and the SBC which are caused by the discrete particle mesh.

Due to the observed deviations of the stress results obtained from the MOP in the Eulerian and the Lagrangian frames, only results computed in the Eulerian frame will be presented in the remainder of this thesis. This is more consistent since the presence of the membranes is felt by the fluid only through the forces in the *Eulerian* frame.

Fig. 9.2(a) nicely shows that the local total stress (sum of fluid and particle stresses) is indeed not a function of the transverse coordinate z. Additionally, its value equals these obtained from the wall stress and Batchelor's approach. This is convincing evidence that the MOP actually provides access to the local particle stress *independently* from assumptions based on macroscopic considerations. Without the MOP, there would be no access to the local particle stress[4]. Instead, one may use Batchelor's approach to find the integrated particle stress for the capsule and localize it at the capsule's centroid position ($z = 15$). This, however, would lead to a single data point in the middle of the flow, and the total stress would not be constant (Krüger et al. [233]).

The local viscosity of the suspension is shown in fig. 9.2(b). For regions filled with fluid only, the

[4]Local means stress averaged over the xy-plane as function of z.

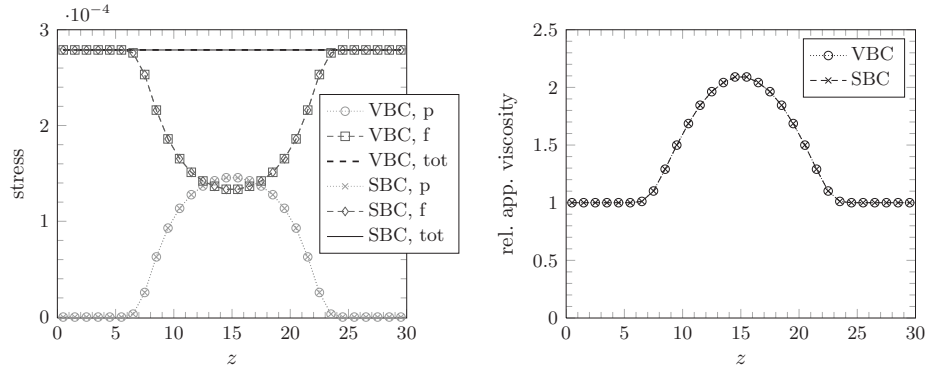

(a) local stresses (b) local viscosity

Fig. 9.2.: Stresses and viscosity for a single capsule. (a) The local, time-averaged stress contributions in steady state are shown for the velocity boundary condition (VBC) and the shear stress boundary condition (SBC). The particle stresses are computed with the MOP in the Eulerian frame. The total stress (sum of particle and fluid stresses) is a constant line, reflecting the condition of mechanical stability. (b) The local, time-averaged relative apparent viscosity is shown. In the fluid region, it is unity as expected. The presence of the particle in the center region (between $z = 7$ and $z = 23$) gives rise to a finite particle stress and increases the viscosity. Curves for VBC and SBC cannot be distinguished in (a) and (b). All time averages are taken between $t = 4000$ and $t = 10000$.

viscosity equals the suspending fluid viscosity. The presence of the particle, however, increases the local viscosity.

9.5.2. Dense suspension in shear flow

In this section, the capability of the wall roughening (section 8.8) in combination with the stress evaluation is demonstrated. Four simulations have been performed: two with rough and two with smooth walls (VBC and SBC each). The average volume fraction in the simulations is 0.5 (189 spherical particles with an average radius of 5 and a polydispersity of 20%). Depending on the radius of the particles, different meshes have been used. This way, it is guaranteed that the average edge length $\bar{l}$ is as close as possible to the lattice constant Δx. In total, six different meshes have been employed, the smallest with 320, the largest with 1620 faces. The system size is $60 \times 60 \times 60$, and the LBM relaxation parameter is $\tau = 1$. Two walls at $z = 0$ and $z = 60$ confine the suspension. The remaining simulation parameters are $\kappa_S = 0.1$, $\kappa_\alpha = 1$, $\kappa_B = 0.01$, $\kappa_A = 1$, $\kappa_V = 1$, $\kappa_{int} = 0.05$, and $\kappa_{gl} = 0.1$. First, the system has been initialized as explained in section 8.5. The resulting system was then taken as the initial state for all four simulations mentioned above.

Velocity boundary condition

For the shear rate driven systems (rough and smooth walls), the two walls were instantaneously accelerated to a velocity of ± 0.02. The resulting wall stresses are shown in fig. 9.3(a). It can be seen that the stresses in the system with smooth walls are smaller. The reason is the low-viscosity slip layer at each wall which can maintain most of the imposed strain. As a result, the shear rate in the bulk region is smaller than the average shear rate, cf. fig. 9.4(b). This is a disadvantage because the bulk shear rate cannot be controlled *a priori* when smooth walls are used. The total stresses obtained from the MOP have been averaged between $t = 2000$ and $t = 10000$ and over

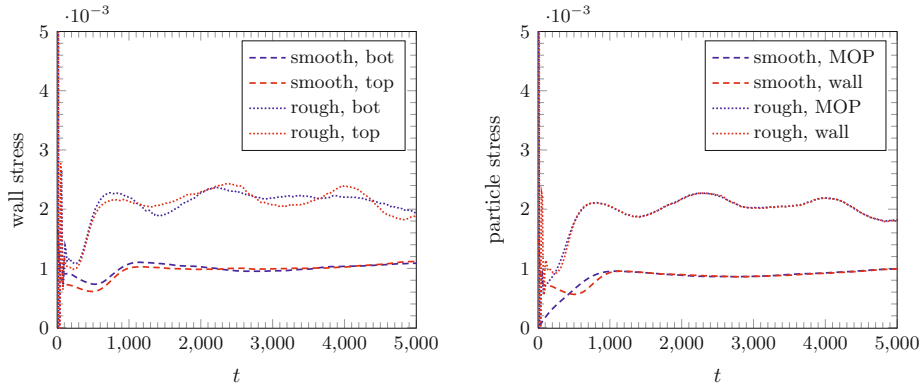

(a) wall stresses (b) particle stresses

Fig. 9.3.: Suspension stresses for rough and smooth walls. (a) For the shear rate driven systems, the resulting wall stresses (bottom and top walls) are presented as function of time. The presence of the slip layers for the smooth walls reduces the stress: The system can be sheared more easily. (b) The particle contribution to the wall stress (averaged over bottom and top walls) is compared with the volume-averaged stress obtained from the method of planes (MOP). After the initial transient in which the fluid is accelerated, both methods yield the same results, even as function of time.

the entire volume: $\langle \sigma_{xz} \rangle_{V,t} = 2.14 \times 10^{-3}$ for the rough and $\langle \sigma_{xz} \rangle_{V,t} = 1.02 \times 10^{-3}$ for the smooth walls. The results obtained from the wall stresses (the bottom and top walls individually) are identical, even if the bottom and top wall stresses are generally not identical at a given time instance, cf. fig. 9.3(a). Batchelor's approach cannot be applied to the system with rough walls because it is not clear how to evaluate the stress related to the roughness force. Still, for the systems with smooth walls, also Batchelor's approach gives the same result for the averaged stress.

In fig. 9.3(b), it is illustrated that the volume-averaged MOP stress matches the average of bottom and top wall stresses even when plotted as function of time. The fluid stress has been subtracted from the wall stresses in order to recover the contribution of the particles. Additionally, the time evolution of the particle stress for the smooth walls obtained from Batchelor's approach matches the corresponding data obtained from the MOP. The curves are identical. Therefore, Batchelor's stress is not shown separately. The transient during the first 1000 time steps in which both stresses are not identical is caused by the required acceleration of the fluid because the fluid is initially at rest. The findings illustrated in fig. 9.3(b) impressively underline that all three methods (wall, MOP, Batchelor) recover the same (volume-averaged) stress as function of time.

Additional results obtained for the simulation with smooth walls are shown in fig. 9.5. In fig. 9.5(a), it is illustrated how important the MOP is for the correct evaluation of the *local* particle stress. If Batchelor's approach is used to compute the stress for each particle individually and then adding this contribution to the z-bin in which the particle center is located, an extremely fluctuating stress profile $\langle \sigma^{\mathrm{p}}_{xz} \rangle_{x,y,t}(z)$ is recovered. The MOP, however, yields the correct stress curve, and the total stress (sum of fluid and particle contributions) are found to be independent of the transverse coordinate z (solid line). For the same simulation, the profiles of the relative apparent viscosity and the local volume fraction are shown in fig. 9.5(b). It can be easily inferred that both Batchelor's stress profile from fig. 9.5(a) and the viscosity are correlated with the volume fraction. Due to the small system size and the short integration time, the averaged density profile shows large fluctuations. In order to extract physically meaningful results, larger systems, longer integration times, and a larger number of independent runs have to be performed,

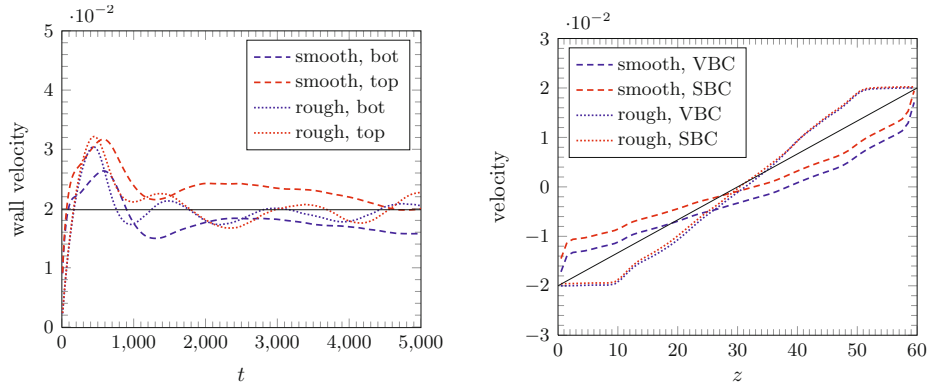

(a) wall velocities (b) velocity profiles

Fig. 9.4.: Suspension velocities for rough and smooth walls. (a) For the shear stress driven systems, the resulting wall velocities (ignoring the minus sign for the bottom wall) are presented as function of time. The time averaged wall velocity (0.02 in all cases) is shown as solid line as reference. (b) The x-components of the velocity (averaged over the xy-plane and times between $t = 2000$ and $t = 10000$) for each simulation run (velocity boundary condition [VBC] and stress boundary condition [SBC]) are shown as function of lateral position z. The low-viscosity slip layers at the smooth walls become noticeable by the localized large velocity gradients. In contrast, for rough walls, there are extended regions (about one average particle diameter) where the velocity is basically constant. The linear velocity profile for the suspending fluid without particles is shown as solid line as reference.

cf. chap. 10. The mere intention of this section is to point out the validity and capability of the stress evaluation methods.

Shear stress boundary condition

For the shear stress driven systems, the imposed stress was chosen to be equal to the resulting stress obtained from the shear rate driven simulations in the interval between $t = 2000$ and 10000. All other simulation parameters have been the same. The resulting wall velocities are shown in fig. 9.4(a). Their averages, also taken between $t = 2000$ and $t = 10000$ give the same velocities as those which have been used for the shear rate driven simulations (± 0.02). This, again, shows the consistency of the SBC, even for rough walls.

Two observations in fig. 9.4(a) have to be explained in more detail: First, the bottom and top walls do not move with the same velocities, not even when averaged over time. The combined average velocity of bottom and top wall, however, yields the expected value of about 0.02. The reason is that, due to the small system size, spatial inhomogeneities are significant, and the viscosity is not the same close to the bottom and top walls. This is also illustrated in fig. 9.5(b). Since the shear rate and not the wall velocity is the relevant quantity, different wall velocities are not problematic as long as the shear rate is correct. Second, one can observe an overshoot of the velocity at $t \approx 500$. This can be understood from the fact that the particles have to be deformed first before they produce significant elastic stresses which decelerate the walls again. The presence of the slip layers, both for the shear rate and the shear stress driven simulations, can be easily inferred from fig. 9.4(b).

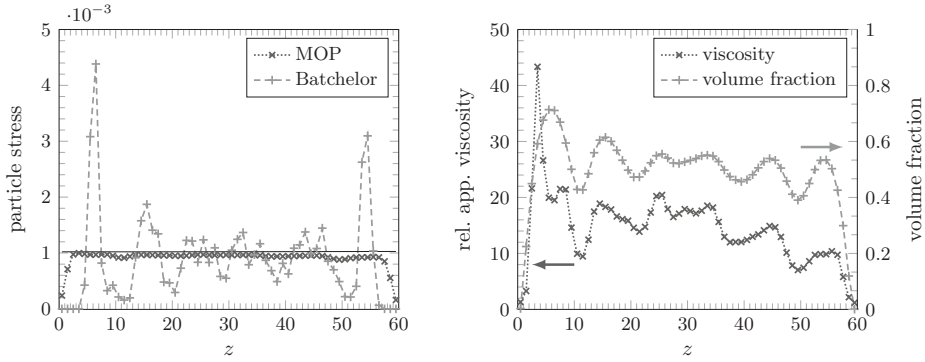

(a) particle stress profiles

(b) viscosity and volume fraction profiles

Fig. 9.5.: Suspension stress, viscosity, and volume fraction profiles. (a) The stresses (averaged between $t = 2000$ and $t = 10000$) for the shear rate driven simulation with smooth walls are shown as function of lateral coordinate z. Batchelor's approach may be used to compute the stress for individual particles and add this contribution to the bin where the particle center is located. This way, a strongly fluctuating particle stress profile is recovered which is clearly correlated to the local density of the particles as shown in (b). Instead, the method of planes (MOP) produces accurate local results for the stress, and the total stress (sum of fluid and particle contributions, solid line) is constant as expected. The results for the remaining three simulations are qualitatively similar and are not shown separately. (b) The local relative apparent viscosity and the local volume fraction for the shear rate driven simulation with smooth walls are shown as function of z. The viscosity and density peaks are obviously correlated.

Conclusions and remarks

The present simulation tool provides the possibility to drive suspensions either by shear rate (via wall velocity) or by shear stress (via wall stress). Independently of this, the walls can be made rough in order to avoid slip. This slip is caused by the presence of the liquid lubrication layers. Although the slip itself is not problematic (walls are present in either case), it is not possible to control the bulk shear rate a priori since the ratio of the viscosity of the lubrication layer and the bulk is not known in advance. The inclusion of the rough walls circumvents this problem.

The stress evaluation approaches (wall, Batchelor, MOP) yield consistent results and complement each other. It has been shown that the fluid and particle contributions to the stress can be computed locally (both in space and time). This opens the door for the analysis of spatio-temporal stress fluctuations which carry important information about the statistical properties of the system. The time-averaged stresses recover the behavior expected for a steady flow.

For all the above simulations, a zero shear stress boundary condition has been used for the y-direction (vorticity axis) at the bottom and the top wall. In particular, this means that the total momentum of the suspension in y-direction is always conserved because the momentum of the fluid can only change due to the influence of external forces like gravity (which is not the case here) or to shear stresses at the walls. Indeed, the y-component of the total fluid momentum was found to be constant up to machine precision, which is another strong indication for the proper functioning of the SBC. As a consequence the 'center of mass' of the fluid does not move along the y-axis when the initial momentum along this axis is zero. This is of paramount importance for the study of particle diffusivities (section 10.7) because undesired superimposed drift velocities may hamper the analysis otherwise.